THE PUBLISHING HOUSE
OF THE ROMANIAN ACADEMY

PROCEEDINGS OF THE ROMANIAN ACADEMY, Series A,
Volume 7, Number 1/2006, pp. 000-000

NUMERICAL ANALYSIS OF THE CAVITATING FLOWS

Sandor BERNAD*, Romeo SUSAN-RESIGA**, Sebastian MUNTEAN*, Ioan ANTON**[#]

*Center of Advanced Research in Engineering Sciences, Romanian Academy, Timisoara Branch, 300223, Timisoara
**Department of Hydraulic Machinery, "Politehnica" University of Timisoara, 300222 Timisoara, Romania
Corresponding author: Sandor Bernad, Romanian Academy – Timisoara Branch,
Bd. Mihai Viteazul 24, 300223 Timisoara, phone: +40 256 403692, fax: +40 256 403700, email: sbernad@mh.mec.upt.ro

Cavitating flows are notoriously complex because they are highly turbulent and unsteady flows involving two species (liquid/vapor) with a large density difference. These features pose a unique challenge to numerical modeling works. This paper reports recent developments and application studies on Computational Fluid Dynamics (CFD) for cavitating flow. The examples of latest technologies for the solver algorithm, physical models (turbulence and cavitation) and meshing tools are presented. The current effort is based on the application of the recently developed full cavitation model that utilizes the modified Rayleigh-Plesset equations for bubble dynamics and includes the effects of turbulent pressure fluctuations to rotating cavitation in different types of fluid turbomachines. Comparisons with available experimental data are used to assess the accuracy of numerical results.

Key words: cavitation, vapour volume, vapour-liquid interface

NOMENCLATURE

c_p	[-]	pressure coefficient
$\dot{m}$	[kg/(s.m^3)]	inter-phase mass flow rate per unit volume
n_b	[1/m^3]	number of bubbles per unit volume of liquid
p	[Pa]	pressure
r	[m]	Radius, radial coordinate
t	[s]	Time
$\mathbf{u}$	[m/s]	absolute velocity
x	m]	axial coordinate
R	[m]	bubble radius
α	[-]	vapour volume fraction
ρ	[kg/m^3]	density
$\boldsymbol{\omega} = \nabla \times \mathbf{u}$	[1/s]	vorticity
σ	[-]	cavitation number

Subscripts

v	vapour of vaporization
l	liquid
∞	points of large distance from the body
ref	reference point
atm	atmospheric pressure

1. INTRODUCTION

In many engineering applications, cavitation has been the subject of extensive theoretical and experimental research since it has predominantly been perceived as an undesirable phenomenon. This is mainly due to the detrimental effects of cavitation such as erosion, noise and vibrations, caused by the growth and collapse of vapour bubbles.

The ability to model cavitating flows has drawn strong interest in CFD community. It covers a wide range of applications, such as pumps, hydraulic turbines, inducers and fuel cavitation in orifices as commonly encountered in fuel injection systems.

Fluid machinery is a common application where low pressures are routinely generated by the machine action, e.g. on blade surfaces, with a consequent possibility of cavitation. Existence of cavitation is often

[#]) Member of the Romanian Academy

undesired, because it can degrade the device performance, produce undesirable noise, lead to physical damage to the device and affect the structural integrity. Details of the existence, extent and effects of cavitation can be of significant help during the design stages of fluid machinery, in order to minimize cavitation or to account for its effects and optimize the design.

Past several decades have seen considerable research on cavitation and extensive reviews are available in the literature [1], [8], [11]. Different aspects of this complex phenomenon have been explored, including, e.g., cavitation bubble collapse [24] and erosion damage, cavitation acoustics, cloud cavitation [23], [24], and rotating cavitation [3], [4].

Based on the assumption that the flow is inviscid, various numerical methods have been thus far proposed to simulate cavitating fows; the conformal mapping method, the singularity method, and the panel method. The flow around hydrofoil [9], [10], [21] and within a centrifugal impeller [6] could be calculated using these inviscid flow models. Experimental observations have revealed that the cavitation appearance relates closely to the viscous phenomena of the liquid-phase, such as the boundary layer and the vortex motion. Recently, viscous flow models, which regard the cavitating flow as the bubbly flow containing spherical bubbles, were introduced to provide highly accurate calculations. In the viscous flow models, the Navier-Stokes equation including cavitation bubble is solved in conjunction with Rayleigh's equation governing the change in the bubble radius. Kubota et al. [10] analyzed the flows around a hydrofoil by the Finite Diference method, and Bunnell et al. [5] calculated the flow in a fuel injection pump for diesel engines by the control volume method. The predominating regions of high volumetric fraction of bubbles obtained by these methods agree well with the cavitation regions observed experimentally.

To account for the cavitation dynamics in a more flexible manner, recently, a transport equation model has been developed. In this approach volume or mass fraction of liquid (and vapor) phase is convected. Singhal et al. [20], Merkle et al. [14] and Kunz et al. [13] have employed similar models based on this concept with diferences in the source terms. Merkle et al. [14] and Kunz et al. [13] have employed the artificial compressibility method. Kunz et al. [13] have adopted a non-conservative form of the continuity equation and applied the model to diferent geometries. Their solutions are in good agreement with experimental measurements of pressure distributions.

The present work addresses the computational analysis of sheet hydrofoil cavitation. Other types of cavitation that occur with sheet cavitation include cloud and bubble cavitation. Sheet cavitation is very common on hydraulic machinery and the present study was motivated by studying the literature concerning the experimental observations and theoretical aspects. A sheet cavity is characterized by a distinct thin vapour bubble attached to the blade surface. Over the years several models have been developed that describe finite cavities. These are characterized by the manner in which the cavity is terminated.

Two-phase cavitating flow models based on homogeneous mixture approach, with a transport equation for the vapor volume fraction have been included in expert commercial codes such as FLUENT [25]. We first evaluate this model for the benchmark problem of a blunt cavitator, and compare the numerical results with experimental data of Rouse & McNown [17]. We have performed such an evaluation for the hemispherical cavitator in [15]. Second, we address the computational analysis of sheet hydrofoil cavitation. The test case corresponds to a NACA 0009 isolated hydrofoil, where experimental data are available in [7].

We conclude that for steady cavitating flow, the model evaluated in this paper correctly captures the pressure distribution on the hydrofoil.

The current effort is based on the application of the recently developed full cavitation model that utilizes the modified Rayleigh-Plesset equations for bubble dynamics and includes the effects of turbulent pressure fluctuations and non-condensible gases (ventilated cavitation) to rotating cavitation in different types of fluid turbomachines.

2. CAVITATING FLOW MODELING

Cavitating flow are very sensitive to the formation and transport of vapour bubbles, the turbulent fluctuations of pressure and velocity and to the magnitude of non-condensible gases, which are dissolved or ingested in the operating liquid [19], [20].

Numerical simulation of two-phase cavitating flows is an ongoing research effort with the ambitious goal to compute the unsteady evolution for cavities grow and collapse. The CFD community has developed so far a set of mature techniques for simulating single-phase viscous flows, and the past half century of accumulated experience may very well serve to shape the numerical cavitating flow research. Early studies rely on the potential flow theory [16]. This approach is now able to correctly describe partially cavitating two-dimensional hydrofoils, including the re-entrant jet cavity closure model [12]. However, extension to 3D problems and other types of cavitating flows seems to be out of reach for the potential flow model.

Although basic cavitation theoretical studies deal with bubble (or bubble clouds) dynamics by solving for the vapour-liquid interface, most of the practical cavitating flows are approached using a homogeneous flow theory. The main idea is to consider a single variable density fluid, without explicit phase interfaces. This model has emerged after carefully examining available experimental investigations, as well as by evaluating the computational costs involved in cavitating flows modelling. A review of cavitating flows numerical studies over the past decade can be found in [23], where various Reynolds Averaged Navier-Stokes (RANS) solvers have been modified to account for the secondary phase (vapour and gas) dynamics.

The mixture model is used in the current work for the numerical simulation of cavitating flows with the FLUENT expert code [25]. In this model, the flow is assumed to be in thermal and dynamic equilibrium at the interface where the flow velocity is assumed to be continuous.

The *mixture* is a hypothetical fluid with variable density,

$$\rho_m = \alpha \rho_v + (1-\alpha)\rho_l \ , \tag{1}$$

ranging from liquid density for $\alpha = 0$ to vapour density ρ_v for $\alpha = 1$. The vapour volume fraction

$$\alpha = \frac{Vol_{vapor}}{Vol_{liquid} + Vol_{vapor}} \ , \tag{2}$$

is an additional unknown of the problem. The mixture will of course satisfy the continuity equation

$$\frac{d\rho_m}{dt} + \rho_m \nabla \cdot \mathbf{u}_m = 0 \, , \tag{3}$$

where d / dt denotes the material derivative. Next, one has to consider a momentum equation for the mixture. A simple choice would be to neglect the viscous effects and use the Euler equation. The system of equations can be then closed with a relationship density-pressure (equation of state). This approach can take advantage of a reach legacy of inviscid compressible solvers [22]. However, when considering a barotropic mixture, i.e. the density depends solely on the pressure, some physics is lost. This can be easily seen when writing the vorticity transport equation

$$\frac{\partial \boldsymbol{\omega}}{\partial t} + \mathbf{u} \cdot \nabla \boldsymbol{\omega} = \boldsymbol{\omega} \cdot \nabla \mathbf{u} + \frac{1}{\rho^2} \nabla \rho \times \nabla p + \text{viscous terms} \ . \tag{4}$$

The second term in the right-hand-side, which accounts for the baroclinic vorticity generation, vanishes when $\rho = \rho(p)$. As a results, an important vorticity source is lost, especially in the cavity closure region [19].

Practical computations of industrial flows are using RANS equations with various turbulence modelling capabilities. This approach is embedded in most commercial codes currently available, e.g. FLUENT [25]. As a result, it seems natural to build a cavitating flow model on top of such computational infrastructure.

An alternative to the equation of state is to derive a transport equation for the vapour volume fraction. The continuity Eq. (3), together with Eq. (1), give the velocity divergence as

$$\nabla \cdot \mathrm{u}_m = -\frac{1}{\rho_m}\frac{d\rho_m}{dt} = \frac{\rho_l - \rho_v}{\rho_m}\frac{d\alpha}{dt} \ . \tag{5}$$

Using Eq. (5), the conservative form of the transport equation for α can be easily written,

$$\frac{\partial \alpha}{\partial t} + \nabla \cdot (\alpha \, \mathrm{u}_m) = \frac{1}{\rho_v}\left[\frac{\rho_v \, \rho_l}{\rho_m}\frac{d\alpha}{dt}\right] . \tag{6}$$

Eq. (6), can be also written for the liquid volume fraction, $1-\alpha$,

$$\frac{\partial (1-\alpha)}{\partial t} + \nabla \cdot [(1-\alpha)\mathrm{u}_m] = \frac{1}{\rho_l}\left[-\frac{\rho_v \, \rho_l}{\rho_m}\frac{d\alpha}{dt}\right] . \tag{7}$$

The factor in square brackets in the r.h.s. of Eqs. (6) and (7) is the interphase mass flow rate per unit volume:

$$\dot{m} = \frac{\rho_v \, \rho_l}{\rho_m}\frac{d\alpha}{dt} \ . \tag{8}$$

If we add term by term Eqs. (6) and (7), we end up with an inhomogeneous continuity equation of the form

$$\nabla \cdot \mathrm{u}_m = \dot{m}\left(\frac{1}{\rho_v} - \frac{1}{\rho_l}\right), \tag{9}$$

which is used in [11] to replace homogeneous Eq (3).

Finally, the vapour volume fraction transport equation is written as:

$$\frac{\partial \alpha}{\partial t} + \nabla \cdot (\alpha \, \mathrm{u}_m) = \frac{1}{\rho_v}\dot{m} \ . \tag{10}$$

This is the equation for the additional variable α, to be solved together with the continuity and momentum equations.

Most of the efforts in cavitation modelling are focused on correctly evaluating $\dot{m}$. One approach has been proposed by Merkle et al. [14], by modelling the phase transition process similar to the chemically reacting flows. This model was successfully employed by Kunz et al. [13] in a variety of cavitating flows. However, the model constants are chosen somehow arbitrary, and this choice ranges several orders of magnitude from one problem to another. Senocak and Shyy attempt a derivation of an empiricism-free cavitation model [19] in order to avoid the evaporation/condensation parameters introduced by Merkle.

A different approach is proposed by Schnerr and Sauer [18], who consider the vapour-liquid mixture as containing a large number of spherical bubbles. As a result, the vapour volume fraction can be written as

$$\alpha = \frac{n_b \frac{4}{3}\pi R^3}{1 + n_b \frac{4}{3}\pi R^3} \ , \tag{11}$$

where the number of bubbles per volume of liquid, n_b, is a parameter of the model.

From (11) we can easily get

$$\frac{d\alpha}{dt} = \alpha(1-\alpha)\frac{3\dot{R}}{R} \ , \tag{12}$$

where $\dot{R}$ is the bubble vapour-liquid interface velocity. A simplified Rayleigh equation can be used to compute

$$\dot{R} \equiv \frac{dR}{dt} = \mathrm{sgn}(p_v - p)\sqrt{\frac{2}{3}\frac{|p_v - p|}{\rho_l}} \ . \tag{13}$$

Of course the bubble grows if the mixture pressure is less than the vaporization pressure, $p < p_v$, and collapses when $p > p_v$. The bubble collapse, as modelled by the Rayleigh second order differential equation, is much more rapid than the bubble growth. However, the above model seems to make no such difference between grow and collapse.

The present paper employs the mixture model, as implemented in the FLUENT commercial code, with the cavitation model described by Eqs. (8), (12) and (13).

Physically, the cavitation process is governed by thermodynamics and kinetics of the phase change process. The liquid-vapor conversion associated with the cavitation process is modeled through two terms, which represents, respectively, condensation and evaporation. The particular form of these phase transformation rates forms the basis of the cavitation model.

3. THE NUMERICAL APPROACH

To simulate the cavitating flow the numerical code FLUENT [25] was used. The code uses a control-volume-based technique to convert the governing equations in algebraic equations that can be solved numerically. This control volume technique consists of integrating the governing equations at each control volume, yielding discrete equations that conserve each quantity on a control-volume basis. The governing integral equations for the conservation of mass and momentum, and (when appropriate) for energy and other scalars, such as turbulence and chemical species, are solved sequentially. Being the governing equations non-linear (and coupled), several iterations of the solution loop must be performed before a converged solution is obtained. The flow solution procedure is the SIMPLE routine [25]. This solution method is designed for incompressible flows, thus being implicit. The full Navier-Stokes equations are solved. The flow was assumed to be steady, and isothermal. In these calculations turbulence effects were considered using turbulence models, as the k-ε RNG models, with the modification of the turbulent viscosity for multiphase flow. To model the flow close to the wall, standard wall-function approach was used, then the enhanced wall functions approach has been used to model the near-wall region (i.e., laminar sublayer, buffer region, and fully-turbulent outer region). For this model, the used numerical scheme of the flow equations was the segregated implicit solver. For the model discretization, the SIMPLE scheme was employed for pressure-velocity coupling, second-order upwind for the momentum equations, and first-order up-wind for other transport equations (e.g. vapor transport and turbulence modeling equations). Computational domain is discretized using the GAMBIT preprocessor [25]. The flow close to the body surface is of particular importance in the current study, the mesh structure in the computational domain deliberately reflects this concern by heavily clustering the mesh close to the solid surface of the body so that the boundary layer mesh is used encloses the body surface.

4. VALIDATION OF THE CAVITATING FLOW MODEL

Before any attempt of computing cavitating hydrofoil flows, we have tested the model described in Section 2 on a benchmark problem. In a previous paper [15] we have computed the cavitating flow over a hemispherical body, with a good agreement witch data a Rouse & McNown [17]. In this paper we analyse the more difficult case of a blunt cavitator. The flow with and without cavitation computed for the axi-symmetric cavitator with blunt fore-body and numerical results are compared with experimental data. For this particular axisymmetric body, Rouse and McNown [17] have provided the pressure coefficient distribution along the body.

In Figure 1, field liquid volume fraction contours and the computational grid are illustrated for the σ = 0.4 case. The results include steady-state computations of non-cavitating and cavitating flows. From the physical point of view, the steady-state assumption is sensible for sheet cavitation, which has a quasi-steady behavior, with most of the unsteadiness localized in the rear closure region [16].

The inlet boundary condition is specified velocity, using a constant velocity profile. Upper and lower boundaries are slip walls, i.e a symmetry condition. The outlet used is a constant pressure boundary

condition. The cavitator itself is no-slip wall. The inlet velocity is set to 1 m/s. This is in the same range as the experimental data.

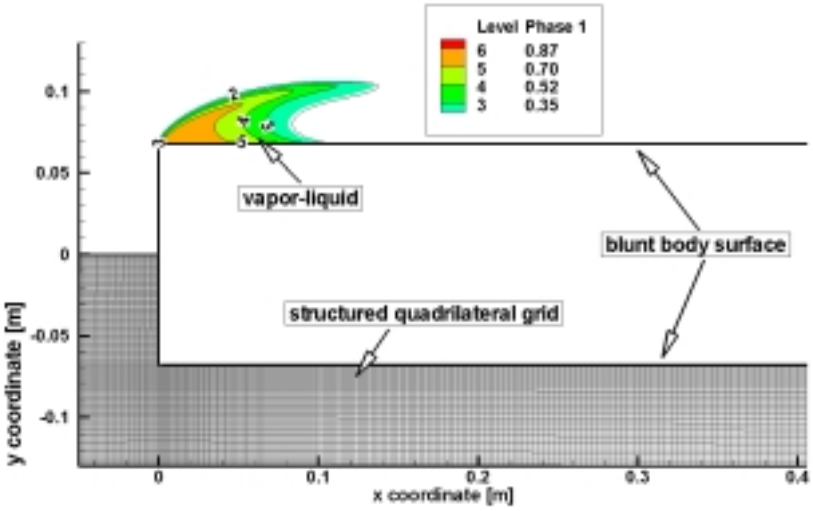

Figure 1. Predicted liquid volume fraction and surface pressure contours, selected streamlines and computational grid for a blunt-body, at cavitation number σ = 0.4.

Figure 1 shows the distribution of α around a hemispherical fore-body, for a cavitation number

$$\sigma = \frac{p_\infty - p_v}{\frac{1}{2}\rho_l U_\infty^2} = 0.3 \tag{14}$$

Most of the computational domain constrains only liquid, $\alpha = 0$, but within the region with $p < p_v$ the vapour phase is formed with $0 < \alpha < 1$.

Cavitation occurs as a result of the flow acceleration over the body surface resulting in regions with pressures lower than the vapor pressure. Then the water transform to vapor in these regions, thereby forming vapor-filled cavities. These cavities collapse when the local pressure becomes larger than vapor pressure, with a reentrant water jet and the flow generally becomes unsteady. Thus an irregular cyclic process of bubble formation and growth occurs, followed by the filling and finally breaking off of the bubble. Due to cavitation, large density and viscosity gradients arise at the interfaces between nearly incompressible fluids.

Within the cavity there are regions practically filled with gas (the first half), and regions with a gas-liquid mixture corresponding to the re-entrant jet dispersion and vaporisation, Figure 2.

The present simulation considers a steady flow, corresponding to a stable attached cavitation. However, when the re-entrant jet crosses the cavity boundary a large part of the cavity detaches and is transported downstream, while the remaining part starts growing again.

Visualisations of the velocity field show the development of a re-entrant jet along the hydrofoil, which is in agreement with the classical theory explaining the periodic shedding of vapour structures downstream from a cavity [10], [12], [13]. The qualitative analysis of the re-entrant jet formation is shown in Figure 3.

The cavity closure is the region where the external flow re-attaches to the wall. The flow which originally moves along the cavity has locally the structure of a jet impinging obliquely upon the wall. The falling stream divides into two parts flowing parallel to the wall. One is the re-entrant jet which moves upstream towards the cavity detachment. The other one makes the flow re-attach to the wall.

The complexity of the problem regarding the region downstream of the cavity is such that all numerical models must introduce some simplifications. The cavity closure region is in fact a two-phase, turbulent zone where vapourization and condensation generate unsteadiness and instabilities. However, for certain flow configurations, the cavity end-zone is only moderately perturbed, thus allowing for a steady solution.

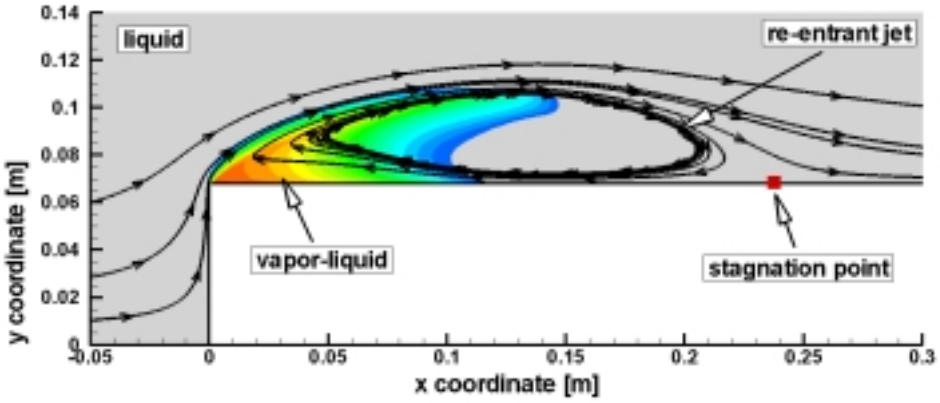

Figure 2. Vapour volume fraction ad selected streamlines for cavitating flow around a blunt fore-body for $\sigma = 0.4$

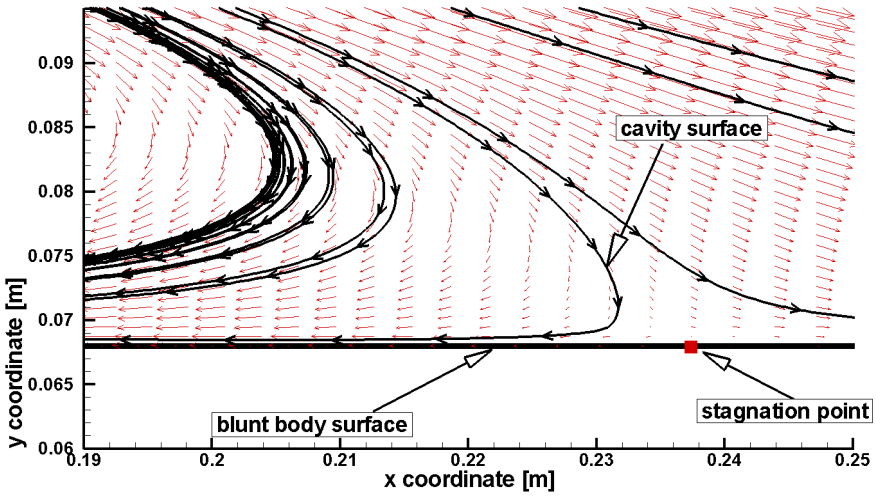

Figure 3. Velocity vector field on the cavity end-zone showing the re-entrant jet formation under cavitating condition for blunt fore-body at $\sigma = 0.3$

It was widely assumed that the character of the cavity termination model only affected the local behaviour of the flow for sufficiently long cavities. However, as observed by Li [8] the cavity shape and length can depend critically upon the termination model and the cavity detachment point.

The pressure coefficient is plotted against the dimensionless curvilinear abscissa along the body, originating at the axis,

$$c_p = \frac{p - p_\infty}{\frac{1}{2}\rho_l U_\infty^2} \tag{15}$$

Figure 4 shows predicted and measured surface pressure distributions at several cavitation numbers for a blunt fore-body with cylindrical afterbody. The model is seen to accurately capture the bubble size as manifested by the decrease in magnitude and axial lengthening of the suction peak with decreasing cavitation number. Also captured is the overshoot in pressure recovery associated with the local stagnation due to bubble closure.

The numerical results correspond to the dashed line, and agree very well with the experimental data [17]. In the cavitation model the vaporization pressure is adjusted to obtain the cavitation number $\sigma = 0.3$ or $\sigma = 0.5$. As a result, the negative values of pressure coefficient are limited within the cavity at $-\sigma$. However, at cavitation inception (upstream and of the cavity) the pressure coefficient still drops below $-\sigma$

as the bubbles are transported faster than they can grow. At the end of the cavity there is a sharp increase in c_p, corresponding to the exact location of the downstream stagnation point from Figure 3.

A number of $n_b = 10^7$ bubbles per unit of liquid volume, Eq. (11) have been used in this simulation. Our numerical experiments have shown that the n_b value does not modify the results for steady flows even if is reduced by an order of magnitude. However, for unsteady flow simulation this is not true.

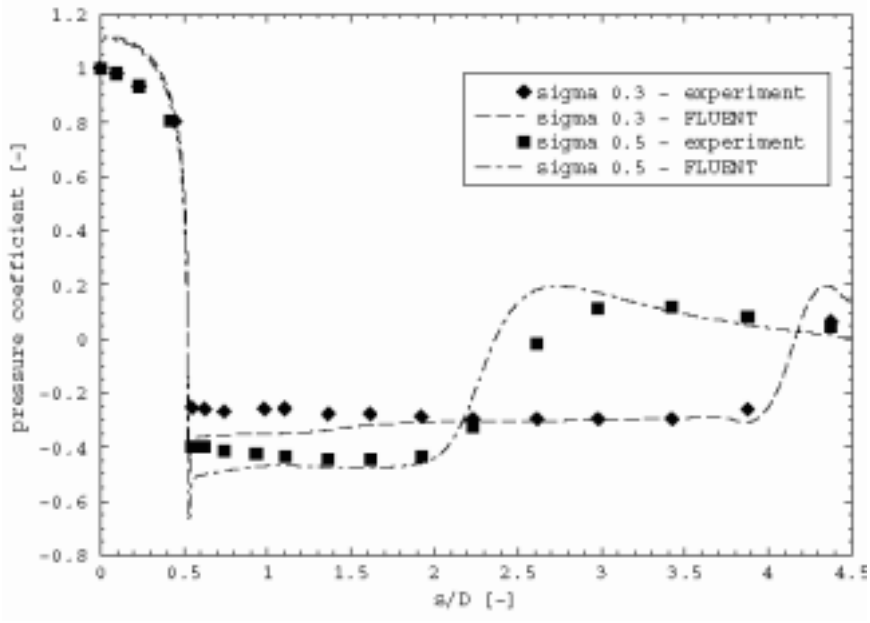

Figure 4. Comparison of predicted and measured surface pressure distributions at several cavitation numbers for a blunt-body (experimental data of Rouse and McNown [15]).

3. CAVITATING FLOW OF A NACA 0009 HYDROFOIL

In this section we examine the fully-wetted flow and the partially cavitating flow for two-dimensional hydrofoils. The main reason for focusing on two-dimensional flow is that particular attention will be given to the method of simulating the flow at the end of the cavity which is a highly turbulent zone characterized by two-phase flow, unsteadiness and instabilities. Thus the rationale is to formulate an accurate model to simulate the two-dimensional flow prior to extending to three dimensions. Most cavity closure models have been formulated to comply with the theoretical analysis of the cavitating flow problem while at the same time attempting to model the physical reality.

The first case we shall present is that of a NACA 0009 hydrofoil at 2.5^0 angle of attack and a cavitation number equal to 0.81, investigated experimentally in [7]. The computational domain is consistent with the experimental setup presented by Dupont [7]. A structured quadrilateral mesh is used for computational domain discretization. Most of the cells are located around the foil, and a contraction of the grid is applied in its upstream part, to obtain an especially fine discretization of the areas where cavitation is expected, Figure 6a.

Standard boundary conditions for incompressible flow are applied: the velocity is imposed at the inlet (V_{ref} = 20 m/s in the present case) and the pressure is fixed at the domain outlet. Then, the pressure is lowered slowly at each new time-step, down to the value corresponding to the desired cavitation number σ defined as $(P_{downstream}-P_{vap})/(\rho_{ref}V_{ref}^2/2)$. Vapor appears during the pressure decrease. The cavitation number is then kept constant throughout the computation.

The presence of a boundary layer will modify the main flow streamlines and subsequently the pressure distribution along the guiding surface. It is important however to distinguish between a cavitation pocket

which forms when the liquid detaches itself from the guiding surface, leaving a liquid-free zone, and a separation pocket which forms when the boundary layer separates, leaving a liquid-filled zone. In nearly all cases, the initial point of separation will occur downstream from the point of minimum pressure as the flow up to this point is accelerating. However, cavitation is caused due to the reaching of a particular absolute pressure at any point in the flow. In general, this absolute pressure will be reached at or very close to the guiding surface. Thus at inception, cavitation will occur close to the point of minimum pressure on the surface.

Experiments have revealed that the location of the cavity detachment point can have a significant effect on the cavity extent and the cavity volume. In the case of a sharp leading edge, the cavity will develop from this point. If however, the leading edge is a smooth curve, the cavity detaches from a point downstream of the laminar boundary layer separation point. The position of the separation and the detachment point and the correlation between them has been studied extensively in literature.

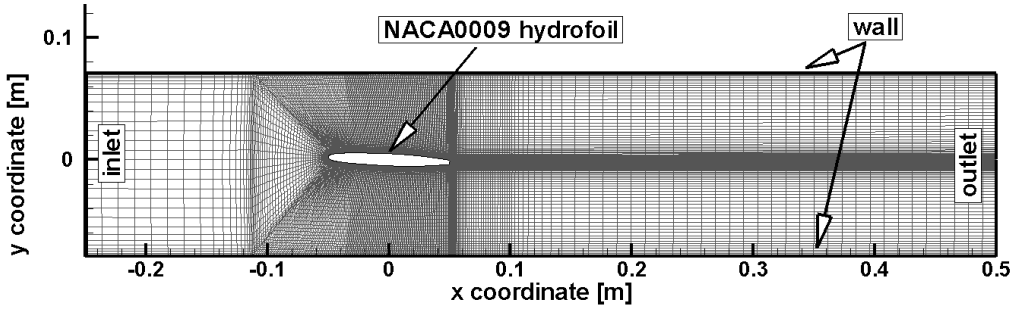

Figure 5. Computational domain and boundary conditions for NACA 0009 hydrofoil.

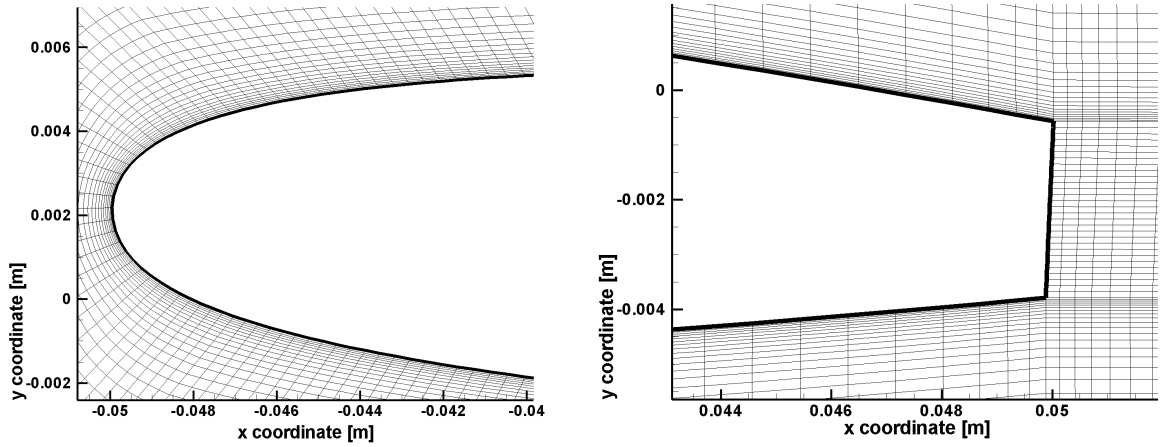

Figure 6. Grid system surrounding the NACA 0009 hydrofoil at 2,5 degree angle of attack; a) A close-up near the leading edge, b) A close-up near the trailing edge.

The gas void fraction contours at the two cavitation numbers are shown in Figure 7. The simulation results indicate the cavity generated on this foil under cavitation number of 0.81 is of stable sheet cavity type. Typical instantaneous pressure contour plots of a cavitating hydrofoil NACA 0009 at non-cavitating and cavitating condition (cavitation number 0.81), are presented in Figures 8, 9 and 10. A region of nearly constant pressure indicating sheet cavity is clearly observable from these figures.

The pressure contours for the flow field at a cavitation number of 0.81 are plotted in Figure 8. We observe that the pressure contours cluster around the cavitation boundary where the density gradient is very large and the flow turns around the cavity.

For the cavitation number of 0.81, the cavity extends up to 30 percent of chord. As the cavitation number increases the gas bubble region decreases in length and comes closer to the surface.

Figure 10b shows the comparison of numerical results with experimental data for both non-cavitating and cavitating flows over an isolated NACA 0009 hydrofoil at $2{,}5^0$ angle of attack. An excellent agreement is obtained between simulation and experiment. Moreover, for cavitating flow we have investigated the effect of turbulence intensity on pressure distribution near the cavity closure. One can see that higher turbulence intensity tends to a sharper cavity closure (dashed line).

Although the incoming turbulence intensity is one order of magnitude smaller in the cavitation tunnel, the turbulence intensity levels considered in the present investigation try to account for the flow induced hydrofoil vibrations.

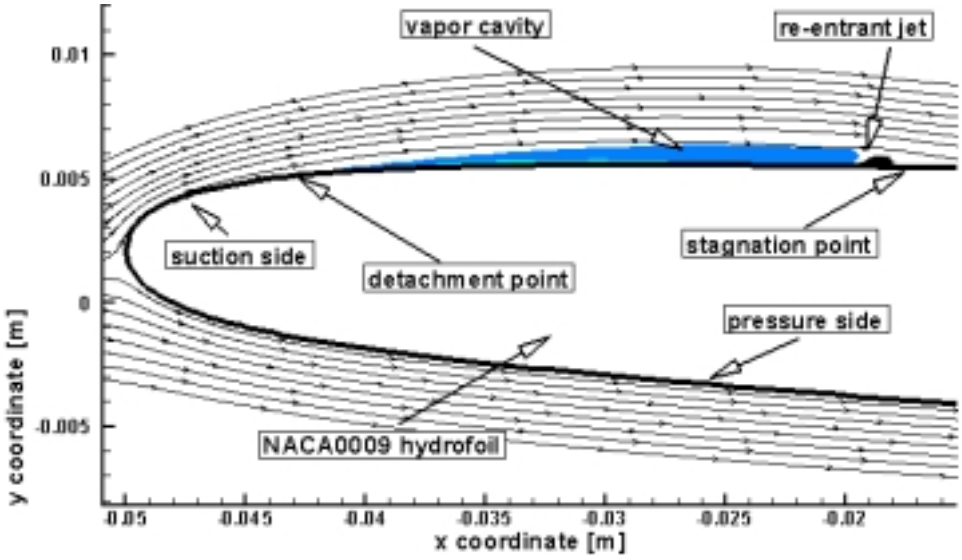

Figure 7. Computed total volume franctions distributions and selected streamlines for NACA 0009 hydrofoil at cavitation number = 0.81.

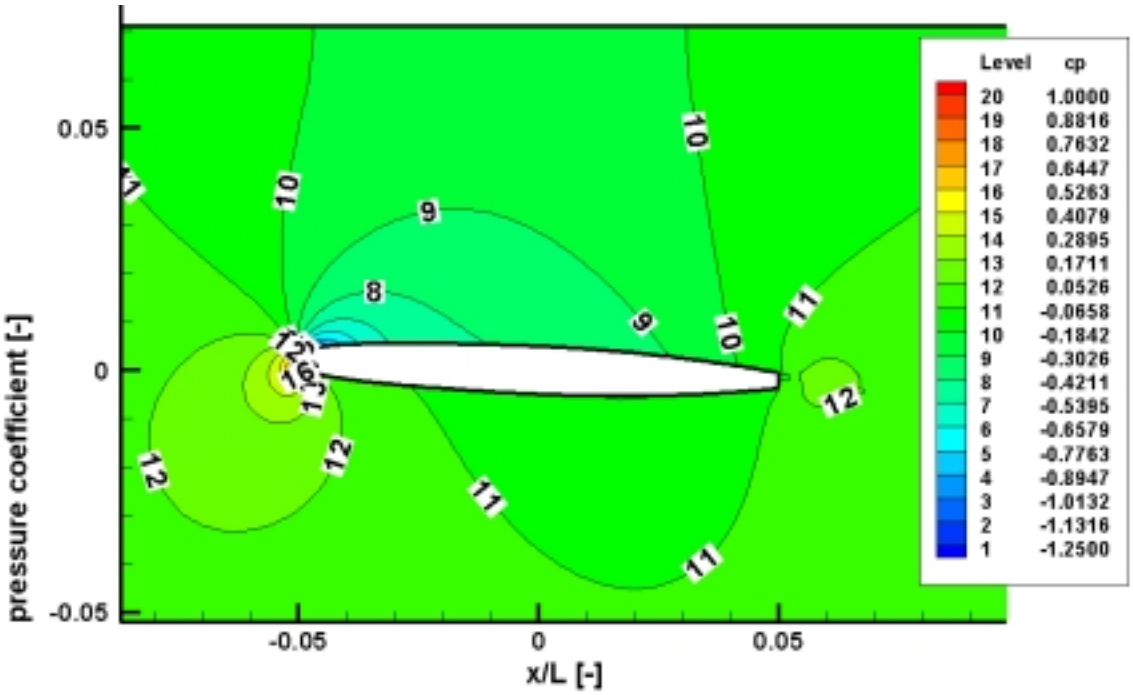

Figure 8. Pressure coefficient distribution on the NACA 0009 hydrofoil at 2,5 degree angle of attack. No cavitation.

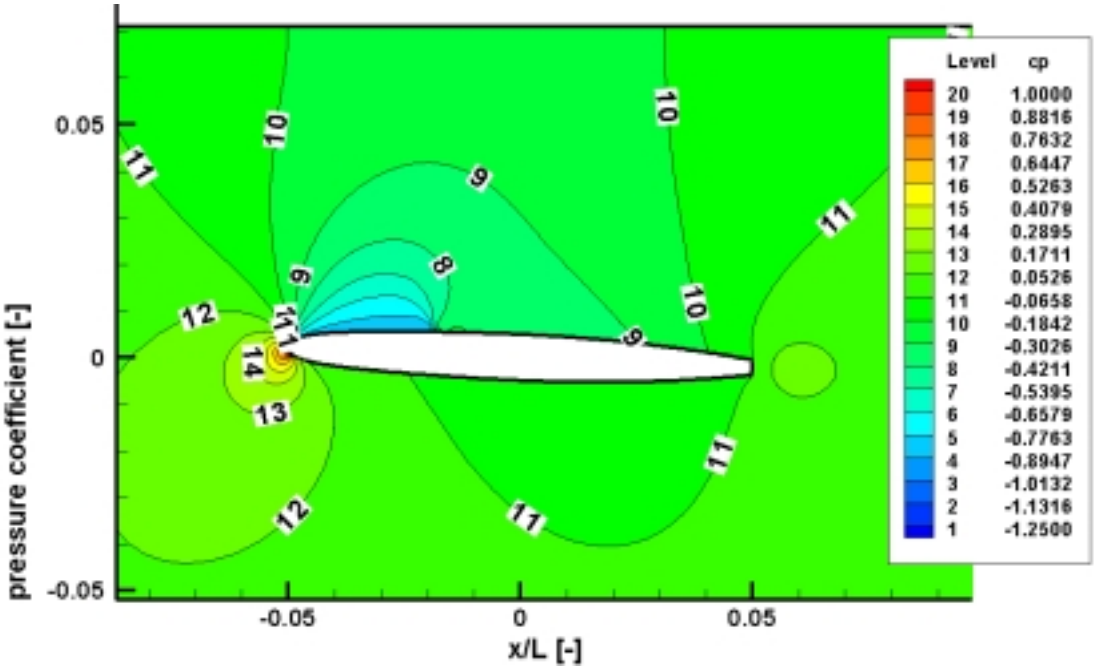

Figure 9. Pressure coefficient distribution on the NACA 0009 hydrofoil at 2,5 degree angle of attack and cavitation number 0.81

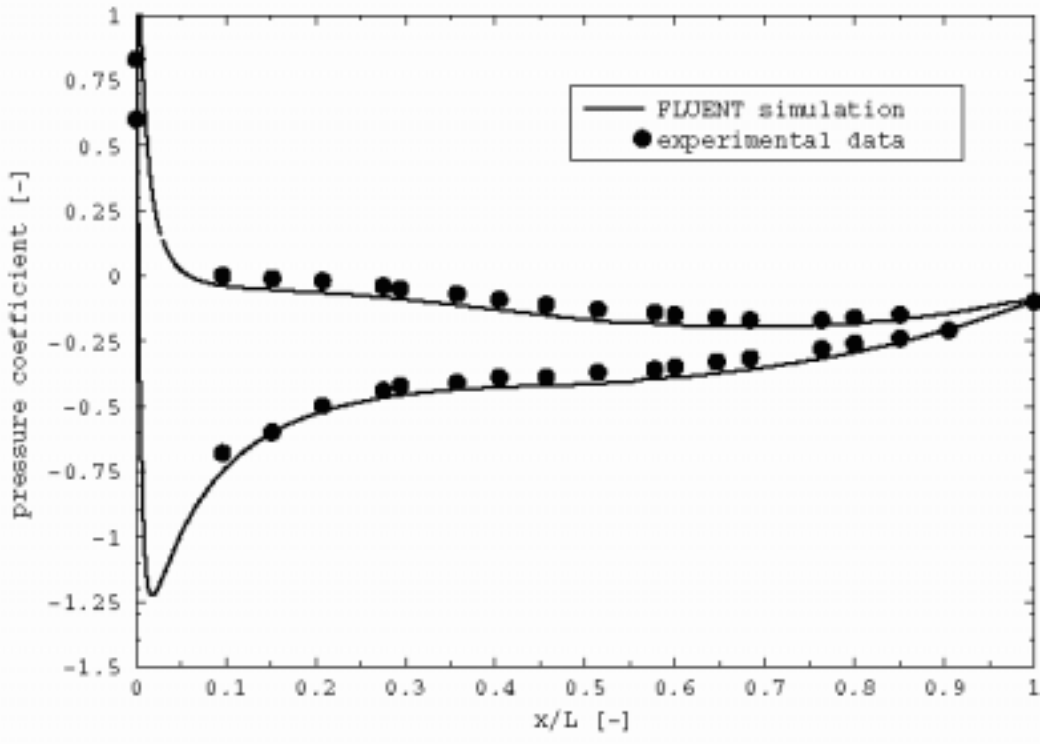

(a)

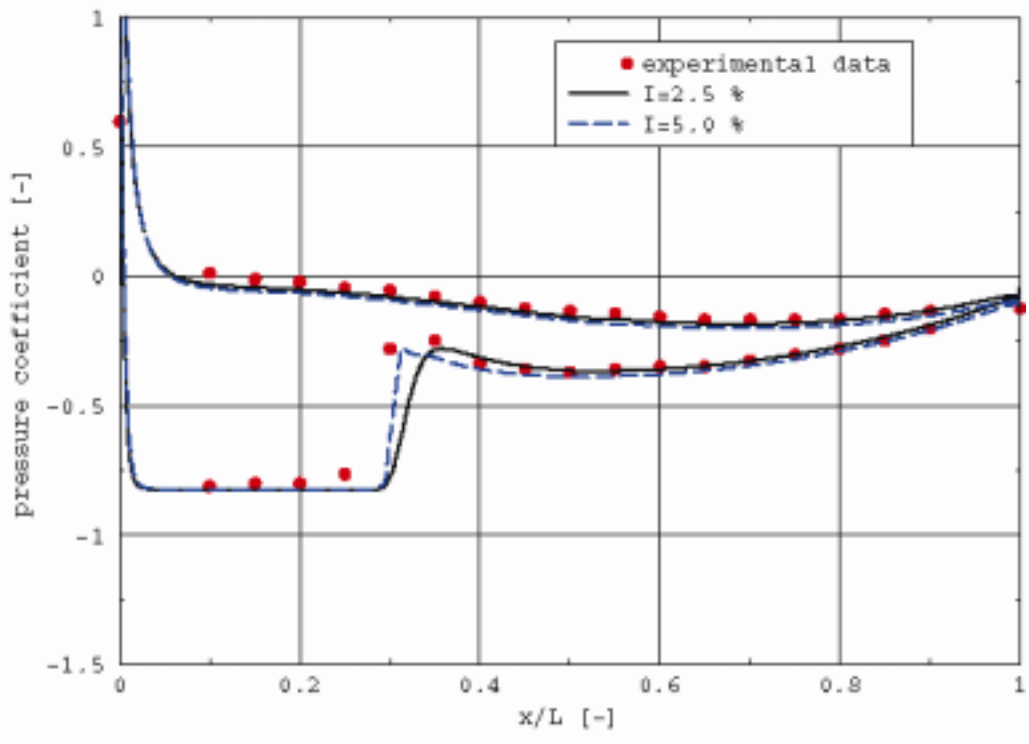

(b)

Figure 10. Pressure coefficient distribution of the different turbulence intensity for NACA 0009 hydrofoil at no-cavitating condition (a) and (b) cavitation number =0.81 (experimental data of Dupont [7]).

5. CONCLUSIONS

The paper presents a numerical investigation of cavitating flows using the mixture model implemented in the FLUENT commercial code [25]. The inter-phase mass flow rate is modelled with a simplified Rayleigh equation applied to bubbles uniformly distributed in computing cells, resulting in an expression for the interphase mass transfer. This is the source term for the vapor phase transport equation. As a result, the density of the liquid-vapor mixture is allowed to vary from the vapor density up to the liquid density.

The cavitation model is validated for the flow around a blunt fore-body cavitator. The numerical results agree very well both qualitatively and quantitatively with the experiments. As a result we include that the present cavitational model is able to capture the major dynamics of attached cavitating flows.

As the authors proceed with this research, we are focusing on several areas including: 1) improved physical models for mass transfer and turbulence, 2) extended application and validation for steady two-dimensional flows.

ACKNOWLEDGMENTS

This work has been supported by Romanian National University Research Council under Grant No. 730/2005. The computation was performed using hardware and software infrastructure on the National Center for Engineering of Systems with Complex Fluids, “Politehnica” University of Timisoara.

REFEREENCES

1. ANTON, I., *Cavitation* (in Romanian), Romanian Academy Publishing House, Bucharest, 1984 (Vol. 1), 1985 (Vol. 2)
2. ARNDT, R. E. A., *Cavitation in Fluid Machinery and Hydraulic Structures*, Ann. Rev. of Fluid Mech., vol. **13**, pp. 273-328., 1981.
3. AVELLAN F., DUPONT P., FARHAT M., GINDROZ B., HENRY P., HUSSAIN M., PARKINSON E., SANTAL O., *Flow survey and blade pressure measurements in a Francis turbine model*. Proceedings of the XV IAHR Symposium, Belgrade, Yugoslavia, Vol. 2, I5, pp. 1-14, 1990.
4. AVELLAN F., DUPONT P., FARHAT M., GINDROZ B., HENRY P., HUSSAIN M., *Experimental flow study of the GAMM turbine model*. In Sottas G. and Ryhming I.L., (eds.), 3D-computation of incompressible internal flows, NNFM 39, pp. 33-53, Vieweg Verlag, Braunschweig, 1993.
5. BUNNELL R.A., HEISTER S.D., *Three-dimensional unsteady simulation of cavitating flows in injector passages*, J. Fluid Eng. vol **122**, pp 791-797, 2000.
6. COUTIER-DELGOSHA O., PERRIN J., FORTES-PATELLA R., REBOUD J.L, *A numerical model to predict unsteady cavitating flow behaviour in inducer blade cascades*, Fifth int. Symp. On Cavitation, Osaka, Japan, 2003.
7. DUPONT P., *Etude de la Dynamique d'une Poche de Cavitation Partielle en Vue de la Prediction de l'Erosion dans les Turbomachines Hydrauliques,* PhDTthesis, These No. 931, EPFL – Lausanne, 1991.
8. Li S.C., *Cavitation of Hydraulic Machinery,* Imperial College Press, 2000.
9. LOHRBERG H., STOFFEL B., FORTES-PATELLA R., COUTIER-DELGOSHA O. REBOUD JL., *Numerical and Experimental Investigations on the Cavitating Flow in a Cascade of Hydrofoils*, Experiments in Fluids, 33/4, pp: 578-586, 2002.
10. KUBOTA A, KATO H., YAMAGUCHI H., *A new modelling of cavitating flows: a numerical study of unsteady cavitation on a hydrofoil section*, J. Fluid Mech., vol. **240**, pp. 59-96, 1992.
11. KUENY, J. L., *Cavitation Modeling,* Lecture Series: Spacecraft Propulsion, Von Karman Institute for Fluid Dynamics, January 25-29, 1993.
12. KRISHNASWAMY, P., *Flow Modelling for Partially Cavitating Hydrofoils*, PhD Thesis, Technical University of Denmark, 2000.
13. KUNZ, R. F., BOGER, D. A., CHYCZEWSKI, T. S., STINEBRING, D. R., AND GIBELING, H. J., *Multi-phase CFD Analysis of Natural and Ventilated Cavitation about Submerged Bodies*, Proc. 3rd ASME/JSME Joint Fluid Engineering Conference, Paper FEDSM99-7364, 1999.
14. MERKLE, C. L., FENG, J. Z., AND BUELOW P. E. O., 1998, *Computational modeling of the dynamics of sheet cavitation*, Third International Symposium on Cavitation, pp: 307-311, 1998.
15. SUSAN-RESIGA, R. F., MUNTEAN S., BERNAD S., ANTON, I., *Numerical investigation of 3D cavitating flow in Francis turbines*, Conference on Modelling Fluid Flow, CMFF'03, Budapest, Hungary, pp: 950-957, 2003.
16. POPP, S., *Mathematical Models in Cavity Theory*, Technical Publishing House, Bucharest, 1985.
17. ROUSE, H., AND MCNOWN, J. S., *Cavitation and Pressure Distribution, Head Forms at Zero Angle of Yaw*, Studies in Engineering Bulletin 32, State University of Iowa, 1948.
18. SCHNERR, G. H., AND SAUER, J., *Physical and Numerical Modeling of Unsteady Cavitation Dynamics*, Proc. 4th International Conference on Multiphase Flow, New Orleans, U.S.A., 2001.
19. SENOCAK, I., AND SHYY, W., *Evaluation of cavitation models for Navier-Stokes computations*, Proceedings of the 2002 ASME Fluids Engineering Division Summer Meeting, Paper FEDSM2002-31011, 2002.
20. SINGHAL, A. K., VAIDYA, N., AND LEONARD, A. D., *Multi-Dimensional Simulation of Cavitating Flows Using a PDF Model for Phase Change*, ASME FED Meeting, Paper No. FEDSM'97-3272, Vancouver, Canada, 1997.
21. SHIN B.R. AND IKOHAGI T, *Numerical analysis of unsteady cavity flows around a hydrofoil*, ASME-FEDSM 99-7215, San Francisco, 1999.
22. VAN DER HEUL, D. R., VUIK, C., WESSELING, P., *Efficient computation of flow with cavitation by compressible pressure correction*, European Congress on Computational Methods in Applied Sciences and Engineering ECCOMAS 2000, 2000.
23. WANG, G., SENOCAK, I., SHYY, W., IKOHAGI, T., AND CAO, S., *Dynamics of attached turbulent cavitating flow*s, Progress in Aerospace Sciences, vol. **37**, pp: 551-581, 2001.
24. WANG, Y-C. AND BRENNEN, C. E., Shock Wave *Development in the Collapse of a Cloud of Bubbles*, ASME FED, Cavitation and Multiphase Flow, vol. **194**, pp. 15–19, 1994.
25. FLUENT 6. User's Guide, Fluent Incorporated, 2002.

Received, October 12, 2005